Terahertz conductivity peak in composite materials containing carbon nanotubes: Theory and interpretation of experiment

G. Ya. Slepyan, M. V. Shuba, and S. A. Maksimenko
Institute for Nuclear Problems, Belarus State University, Bobruiskaya 11, 220050 Minsk, Belarus

C. Thomsen
Institut für Festkörperphusik, Technische Universität Berlin, Hardenbergstr. 36, D-10623 Berlin, Germany

A. Lakhtakia
Nanoengineered Metamaterials Group, Department of Engineering Science and Mechanics, Pennsylvania State University, University Park, Pennsylvania 16802-6812, USA and
Department of Physics, Indian Institute of Technology Kanpur, Kanpur 208016, India

(Received 13 February 2010; revised manuscript received 5 April 2010; published 17 May 2010)

A model for the effective conductivity of a dilute and disordered composite material containing randomly single-wall carbon nanotube (SWCNT) inclusions was formulated. The modification of electron transport by the surface curvature of SWCNTs and an axial depolarization effect due to the finite length of metallic SWCNTs are taken into account. Simultaneous consideration of both effects permits the correct interpretation of the dependences of the effective conductivity on the frequency and temperature, and explains an experimentally observed terahertz peak in the spectrum of the effective conductivity.

DOI: 10.1103/PhysRevB.81.205423 PACS number(s): 42.70.−a, 73.25.+i, 77.84.Lf, 78.67.Ch

I. INTRODUCTION

Carbon nanotubes (CNTs) (Ref. 1)—single- or multiwalled hexagonal networks of carbon atoms rolled up into cylinders—are extensively studied as potential components of high-frequency electronic circuits, such as transmission lines,[2] interconnects,[3] and antennas.[4–11] Much attention is being paid nowadays to the electromagnetic response of composite materials containing CNT inclusions, as these materials are promising as optical and terahertz materials. Although the characteristics of these composite materials are dictated by the properties of isolated CNTs (Ref. 12) but the relationship appears to be nontrivial—as indicated by several experimental reports[13–22] of a broad conductivity peak in the terahertz and the far-infrared regimes displayed by composite films containing CNTs. This peak does not conform to the Drude conductivity model, which was originally expected to be valid below the optical transition band, and thus requires incorporation of additional physical mechanisms.

In general, these mechanisms are related to specific geometric features: either the finite length[6,8,19] or the finite radial curvature of CNTs.[22,23] The curvature of a CNT leads to a modification of the orientations of π orbitals of adjacent carbon atoms and to the modification of the overlap integral. The electron-dispersion relation therefore changes. As depicted qualitatively in Fig. 1, in the vicinity of the Fermi point for conductive CNTs, the relation $\mathcal{E}(p_z)=\pm\upsilon_F|p_z|$ of the Dirac type has to be altered to $\mathcal{E}(p_z)=\pm\sqrt{E_g^2+\upsilon_F^2 p_z^2}$ that indicates a narrow gap; here, $\mathcal{E}$ is the electron energy, p_z is the axial projection of the electron quasimomentum, $2E_g$ is the energy gap, and υ_F is the π-electron speed at the Fermi level. The effect of the narrow gap in Fig. 1 is referred to by us as the curvature effect.

Theoretical analysis[24] suggests that the energy gap $2E_g \cong (3/16)(b/R)^2\gamma_0 \sin(3\varphi)$, where φ is the chiral angle of the CNT, R is the CNT radius, $b=0.142$ nm is the interatomic distance in graphene, and $\gamma_0 \simeq 3$ eV is the overlap integral. Thus, the magnitude $2E_gR^2$ is maximal for zigzag CNTs and $2E_g=0$ for armchair CNTs. For typical narrow-gap CNTs, the frequency $E_g/\pi\hbar$ lies in the vicinity of a conductivity peak in the terahertz and the far-infrared regimes.[23]

An alternative interpretation of the conductivity peak is based on phonon resonance.[20] However, this interpretation contradicts the weak dependence of the peak's parameters on temperature.[18]

Thus, the available physical models agree well with some, but not all, aspects of the available experimental data. However, the correct understanding of the origin of the conductivity peak is important both for modeling isolated CNTs as well as for using composite materials containing CNT inclu-

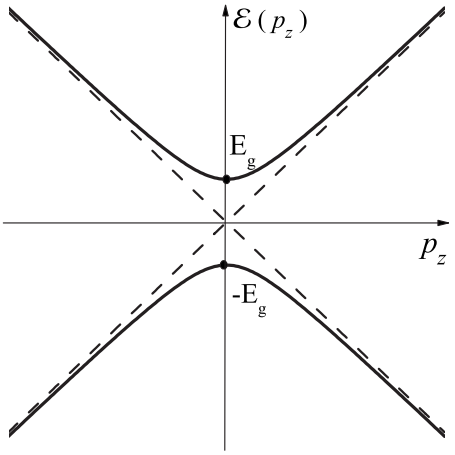

FIG. 1. Solid lines: electron dispersion relation of an otherwise metallic CNT with a narrow gap due to curvature. Dashed lines: electron dispersion relation of the Dirac type. As these schematics are for free π electrons, relaxation is not included.

sions as coatings to reflect/absorb electromagnetic radiation.

In this paper, we present a complete physical picture of the terahertz conductivity peak (TCP)—through a model which addresses both finite length and curvature effects, such that both phenomena are mutually complementary, not competitive. The finite length affects depolarization[25] by a metallic CNT significantly when low-frequency axial plasmon excitations occur, with consequent effects on the effective properties of composite materials containing CNT inclusions. Our model demonstrates good agreement with different experiments over wide temperature and spectral ranges (with the regime of optical quantum transition included).

II. EFFECTIVE-CONDUCTIVITY MODEL

Let us consider a dilute composite material comprising randomly dispersed, randomly oriented, achiral, single-walled CNTs (SWCNTs) of different lengths in free space. The chosen SWCNTs are described by either the dual index $(m,0)$ or the dual index (m,m).[1] We designate the single index j to identify the type of SWCNT. The distribution function $N_j(L)$ describes the number density of SWCNTs of type j and length L. All orientations are equiprobable and f denotes the volume fraction occupied together by the SWCNTs (conceived as cylinders of volume $\pi R_j^2 L$).

Our model requires the calculation of the complex-valued effective conductivity σ_{eff} of the composite material, as function of the angular frequency ω, using two different approaches. Approach A is a long-wavelength approach valid when the length L of all SWCNTs is a small fraction of the free-space wavelength λ. Approach B is a short-wavelength approach that is applicable when finite-length effects vanish.

Approach A. The simple Waterman-Truell formula[26,27] was adopted to estimate the effective refractive index of the chosen composite material as

$$n_{eff}(\omega) \cong \sqrt{1 + \frac{4\pi f}{3k^2}\sum_j \int_0^\infty F_j(0,\omega,L) N_j(L) dL}, \qquad (1)$$

whence $\sigma_{eff}(\omega) = \omega[n_{eff}^2(\omega) - 1]/4i\pi$. Here, $k = 2\pi/\lambda = \omega/c$ is the free-space wave number, $F_j(0,\omega,L) \equiv \lim_{\theta\to 0} F_j(\theta,\omega,L)$, and $F_j(\theta,\omega,L)$ is the plane-wave scattering amplitude of an isolated SWCNT at angle θ with respect to the direction of propagation of a plane wave by an SWCNT of type j and length L. The factor 1/3 in Eq. (1) is due to the random orientations of the SWCNTs, furthermore, as each SWCNT in free space acts as an electric-dipole scatterer,[12] the equality of the backscattering amplitude $F_j(\pi,\omega,L)$ and the forward-scattered amplitude $F_j(0,\omega,L)$ has been incorporated in that expression.

In order to calculate $F_j(0,\omega,L)$, we applied an integral-equation method which relies on the prescription of effective boundary conditions for the electromagnetic field on the surface of a SWCNT.[2,8,9] The axial surface conductivity $\sigma_{zz}^{(j)}(\omega)$ of an SWCNT required for this purpose was calculated with the application of a tight-binding model for π-electron motion that takes spatial quantization into account.[28]

Each SWCNT in free space has an axial polarizability $\alpha_j(\omega,L) = k^{-2} F_j(0,\omega,L)$ in free space. One method to compute $\alpha_j(\omega,L)$ is by solving the integral equation mentioned earlier. A simpler method to compute $\alpha_j(\omega,L)$ is as follows.

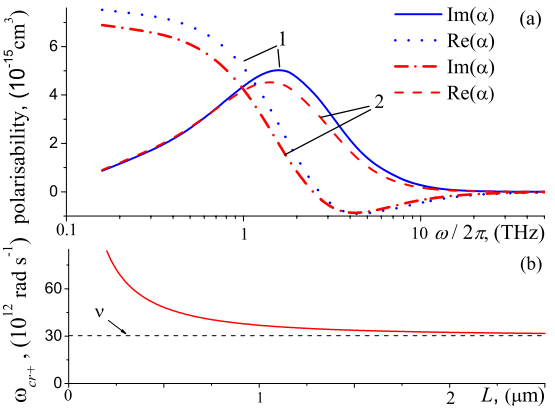

FIG. 2. (Color online) (a) Frequency dependence of the axial polarizability $\alpha(\omega,L)$ of a (24,0) SWCNT of length $L=1$ μm calculated by the integral-equation method (Ref. 6) (lines marked 1) and by Eq. (2) (lines marked 2), when $\nu = 3\times 10^{13}$ rad s^{-1}. (b) Dependence of the crossover angular frequency ω_{cr+} on the length L of a (24,0) SWCNT. The dashed line indicates the electron relaxation angular frequency $\nu = 3\times 10^{13}$ rad s^{-1}.

Suppose that each SWCNT is a prolate spheroid made of an orthorhombic material whose relative permittivity $\varepsilon_{zz}^{(j)} = 1 + (4\pi i/\omega)(2\sigma_{zz}^{(j)}/R_j)$ in the axial direction and whose relative permittivity in any direction normal to the axis equals unity. Neglecting the effect of curvature, we have $\sigma_{zz}^{(j)} = 3i\gamma_0 be^2/\pi^2\hbar^2 R_j(\omega + i\nu)$ so that $\varepsilon_{zz}^{(j)} \approx 1 - (\omega_p^{(j)})^2/\omega(\omega + i\nu)$ for a metallic SWCNT, where ν is the relaxation angular frequency (assumed independent of the SWCNT type) and $\omega_p^{(j)} = (4e/R_j)(v_F/\pi\hbar)^{1/2}$ is the plasma frequency. Then

$$\alpha_j(\omega,L) \cong -\frac{LR_j^2}{6}\frac{(\omega_p^{(j)})^2}{[\omega^2 - (\omega_p^{(j)})^2 n_z^{(j)} + i\omega\nu]}, \qquad (2)$$

where $n_z^{(j)} \approx 4(R_j/L)^2[\ln(L/R_j) - 1]$ and $v_F = 3\gamma_0 b/2\hbar$.

Figure 2(a) shows the frequency dependence of the axial polarizability $\alpha(\omega,L)$ of a (24,0) SWCNT calculated rigorously using the integral-equation method[6] and approximately using Eq. (2). The reasonably good agreement between the two methods justifies the use of Eq. (2) in most of the remainder of this paper.

Approach B. The previous approach to find $\sigma_{eff}(\omega)$ is valid only for $kL < \pi/5$. In contrast, Approach B is independent of L because it is applicable only in the regime of optical transitions, wherein surface-wave propagation in SWCNTs is strongly attenuated[6] and finite-length effects vanish. Therefore, the integral equation for scattering by a SWCNT can be solved using the Born approximation. The effective conductivity of the composite material is then given by

$$\sigma_{eff}(\omega) = (2\pi/3)\sum_j R_j \tilde{n}_j \sigma_{zz}^{(j)}(\omega), \qquad (3)$$

where $\tilde{n}_j = \int_0^\infty N_j(L) dL$. Approach B is thus applicable only at sufficiently high frequencies. We found the spectral regimes of applicability of the two approaches to find $\sigma_{eff}(\omega)$ to

overlap—e.g., in the vicinity of $\lambda=10$ μm for the (24,0) CNT.

III. NUMERICAL RESULTS AND COMPARISON WITH EXPERIMENTAL DATA

Let us now compare results from both approaches with experimental data.[18] For this comparison, we assumed that $N_j(L)\sim\exp[-(L-L_0)^2/\sqrt{2}\Delta]$ is Gaussian and independent of j, with L_0 and Δ to be fixed later.

Now, $\sigma_{eff}(\omega)$ as determined from Eq. (1) appears to conform to an experimentally observed crossover angular frequency ω_{cr} with respect to temperature:[18] $\mathrm{Re}(\sigma_{eff})$ decreases with increasing temperature for $\omega<\omega_{cr}$ but increases with increasing temperature for $\omega>\omega_{cr}$. Indeed, as discussed later, this feature is a general property of composite materials containing inclusions whose conductivities are of the Drude form.

The existence of crossover angular frequencies for the composite material stems from the crossover angular frequencies of a single scatterer. Suppose that ν depends on the temperature T then a crossover angular frequency $\omega_{cr}^{(j)}$ must satisfy the relation $\partial(\mathrm{Im}[\alpha_j(\omega_{cr}^{(j)},T)])/\partial T\sim\partial(\mathrm{Im}[\alpha_j(\omega_{cr}^{(j)},T)])/\partial\nu=0$. By virtue of Eq. (2), we get two crossover angular frequencies

$$\omega_{cr\pm}^{(j)}=\frac{1}{2}\nu[\sqrt{1+4n_z^{(j)}(\omega_p^{(j)})^2/\nu^2}\pm 1]. \tag{4}$$

Figure 2(b) demonstrates the dependence of $\omega_{cr+}^{(j)}$ on the length L. For SWCNTs of length $L>0.8$ μm, the inequality $4n_z^{(j)}(L)(\omega_p^{(j)})^2/\nu^2\ll 1$ holds, which indicates that $\lim_{L\to\infty}\omega_{cr+}^{(j)}=\nu$. This trend is confirmed in Fig. 2(b) and should be reflected in σ_{eff}.

Indeed, when the conductivity of a composite material is of the Drude type, the crossover frequency satisfies the relation $\mathrm{Re}[\sigma_{eff}(\omega_{cr})]=(1/2)\max_\omega\{\mathrm{Re}[\sigma_{eff}(\omega)]\}$, as has been experimentally confirmed.[18] Accordingly, we can conclude that the conductivities of the SWCNT inclusions in the terahertz regime indeed follow the Drude relation.

Using either Approach A or B, as appropriate, and with data from Ref. 18, we calculated $\sigma_{eff}(\omega)$. In this context, let us note that (i) the axial surface conductivity is the same for all types of metallic SWCNTs, whether chiral or achiral, of identical radius [Eq. 24 in Ref. 2] and (ii) $\sigma_{zz}^{(j)}\propto R_j^{-1}$. Therefore, per Eq. (2), the axial polarizability α_j depends very slightly on R_j as $\ln(R_j)$. As all metallic SWCNTs of the same length in a realistic composite material thus have approximately the same axial polarizability, regardless of differences in radius, we did not take variations in R_j into account and instead modeled all metallic SWCNTs as being of a single type. Accordingly, for theoretical purposes, the composite material contains only two types of SWCNTs: metallic ($j=1$) and semiconducting ($j=2$). The ratio of their concentrations is $\tilde{n}_2/\tilde{n}_1=2$.

The samples in Ref. 18 contain SWCNTs of average radius 1.37 nm and mass density 0.4 g cm^3; hence, the volume fraction of metallic SWCNTs is about 0.06. We chose $R_1=1.4$ nm [zigzag (18,0)] and $R_2=1.1$ nm [zigzag (14,0)].

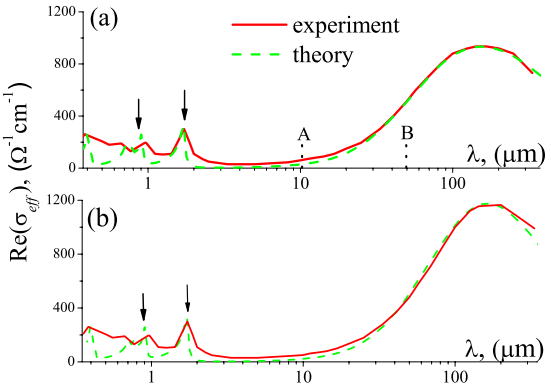

FIG. 3. (Color online) Variations in $\mathrm{Re}(\sigma_{eff})$ with λ at (a) $T=300$ K and (b) $T=50$ K. Solid lines: experimental data from Fig. 3 of Ref. 18. Dashed lines: theoretical results. When the long-wavelength Approach A was used, we set (a) $\nu=3\times10^{13}$ rad s^{-1} and (b) $\nu=2.3\times10^{13}$ rad s^{-1}. When the short-wavelength Approach B was used (in the regime of interband transitions), $\nu=5\times10^{13}$ rad s^{-1}, regardless of the temperature. The TCP is on the right in both figures. Arrows indicate the resonance lines due to the first two optical transitions of semiconducting SWCNTs. In (a), the vertical dotted line identified by the symbol A indicates the smallest wavelength of applicability of Approach A, and the vertical dotted line identified by the symbol B indicates the largest wavelength for which Approach B is valid; both approaches are valid in the wavelength regime between the two dotted lines.

We set ν equal to the experimentally observed[18] crossover angular frequency, when Approach A was used: $\nu\simeq\omega_{cr+}^{(1)}=3\times10^{13}$ rad s^{-1}, at $T=300$ K. The parameters $L_0=1.6$ μm, $\Delta=0.58$ μm, and $\tilde{n}_1=2.63\times10^{16}$ cm^{-3} were chosen to match the frequency, line width, and amplitude of the TCP in the experimental data of Ref. 18.

Figure 3 shows that our theoretical model comprising Approaches A and B for different spectral regimes describes the form of the experimentally observed TCP very well. Besides, the predicted amplitudes of resonance lines due to first two optical transitions of the semiconducting SWCNTs coincide reasonably well with the experimental values. This coincidence is remarkable because we chose L_0, Δ, and $\tilde{n}_1$ *only* to match the experimentally observed TCP. Thus, the value of $\tilde{n}_1$ chosen to implement the long-wavelength Approach A is also germane to the short-wavelength (optical) regime, thereby confirming our ansatz $\tilde{n}_2=2\tilde{n}_1$ that emerged from the equiprobability of SWCNTs of identical radii but different chiral angles.

The bandwidth of the TCP is determined with high accuracy by electron relaxation processes (relaxation linewidth ≈20 meV) and inhomogeneously broadened due to length dispersion in composite materials (≈3 meV). Note that the densities of the model composite material and the realistic composite material of Ref. 18 also coincide.

The conductivity peak observed in Ref. 18 is not related to the localized defect states for three reasons. First, the SWCNTs were baked to decrease lattice defects. Second, localization effects diminish with rising temperature and are significant only at temperatures below 200 K.[29,30] Third, when the temperature ranges between 50 and 300 K, the contribution of localized defect states to the conductivity of a

metallic SWCNT is smaller than that of conduction electrons—as confirmed by the weak temperature dependence of the conductivity in this temperature range.[29,30]

Let us now discuss the reason for the prediction of the TCP by our model. Most importantly, the frequencies of geometrical (antenna) resonances of an SWCNT of the type j are determined by the complex poles of its polarizability $\alpha_j(\omega)$ in Eq. (2). For the first resonance we have $\omega_{res}^{(j)} \cong \pm\sqrt{(\omega_p^{(j)})^2 n_z^{(j)} - \nu^2/4} - i\nu/2$. For parameters corresponding to the experimental data in Ref. 18, we get $\omega_p^{(j)}(n_z^{(j)})^{1/2} < \nu/2$ so that $\omega_{res}^{(j)}$ is imaginary. Considering the SWCNT as equivalent to a series $\mathcal{RLC}$ circuit with inductance $\mathcal{L}_j = 6/L(R_j\omega_p^{(j)})^2$, capacitance $C_j = LR_j^2/6n_z^{(j)}$, and resistance $\mathcal{R}_j = \nu\mathcal{L}_j$, we see that $\mathcal{R}_j > \sqrt{\mathcal{L}_j/C_j}$ and, as a consequence, the power lost to Ohmic dissipation exceeds the reactive power. At the angular frequency $\omega_o^{(j)} = 1/\sqrt{\mathcal{L}_j C_j} = \omega_p^{(j)}(n_z^{(j)})^{1/2}$, the equivalent reactance of the series circuit vanishes, and the long-wavelength peaks appear in Fig. 3. We caution that existence of a peak in the spectrum of $\mathrm{Re}[\sigma_{eff}(\omega)]$ does not imply the existence of an electromagnetic resonance mode. Each resonance mode of an electromagnetic field has a peak in the spectrum of the photonic density of states[31] but this peak does not exist for a mode corresponding to an imaginary frequency.

The TCP emerges from a strong axial depolarization field (that can be considered to be an axial plasmonic effect[19]) for metallic SWCNTs. This reason is supported by the dependence of $\omega_o^{(j)}$ on the depolarization factor $n_z^{(j)}$. Whereas $\omega_o^{(j)}$ depends strongly on the length L through $n_z^{(j)}$, its dependence on the radius R_j is weak (logarithmic). These dependences are in accord with experimental data[19] which show that highly stretch-aligned SWCNTs are collectively characterized by a strong optical anisotropy. Indeed, the usual absorption peak was observed for incident terahertz radiation polarized parallel to the SWCNT axis but not for perpendicular polarization.[19] This discrimination was presented by the authors of Ref. 21 as evidence of the incorrectness of plasmonic explanation. In a later publication,[22] the same authors discussed only the transverse plasmonic effect but omitted the axial plasmonic effect due to the small value of $n_z^{(j)}$. However, the reverse is actually true. A metallic SWCNT has a significant axial plasma frequency $\omega_p^{(j)}$ that leads to a value of $\omega_o^{(j)}$ corresponding to experimental data while the transverse plasmonic effects are vanishingly small.

The alternative interpretation of the TCP available in the literature stems from the quantum transition of π electrons through the narrow gap.[13,15,22,23] A simpler model[22] is based on the description of the CNT-containing composite material as a two-level system with levels placed on the top of valence band and on the bottom of the conduction band and transition angular frequency $2E_g/\hbar$. This interpretation contradicts the principles of quantum mechanics for the following reason. π electrons are not free particles and interact with the reservoir, as encapsulated by the relaxation angular frequency. Weak interactions ($2E_g \gg \hbar\nu$) can be described by the concept of two quasidiscrete levels.[31] Each level has a narrow peak in the spectrum of the electron density of state. The dynamics of the system are governed chiefly by quantum transitions between the two quasidiscrete levels. However, if the interaction increases (i.e., ν increases), both peaks broaden and overlap more. When $2E_g < \hbar\nu$—which holds true for the experimental data provided in Ref. 18—both peaks coalesce into one peak appearing at $\mathcal{E}=0$. This means that strong interaction with reservoir suppresses the effect of the narrow gap and the gap is practically transformed into an allowed band. Thus the TCP is mainly caused by the quasiclassical motion of π electrons in the vicinity of the Fermi point $\mathcal{E}=0$.

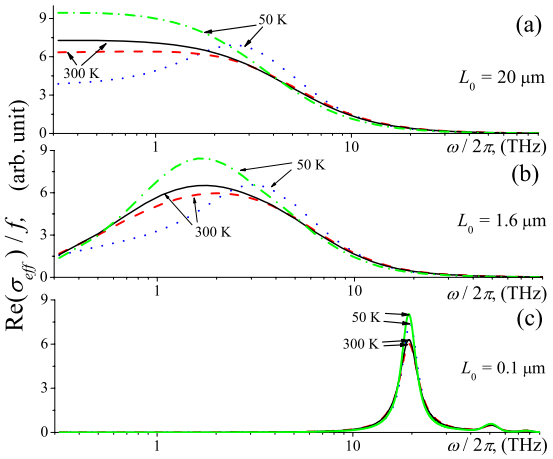

FIG. 4. (Color online) Frequency dependence of $\mathrm{Re}(\sigma_{eff})/f$ of a composite material comprising identical zigzag (27,0) SWCNTs: (a) $L_0=20$ μm, (b) $L_0=1.6$ μm, and (c) $L_0=0.1$ μm. Note that $\mathrm{Re}(\sigma_{eff}) \sim f$ for $f \ll 1$. The curvature effect was taken into account at both $T=50$ K (dotted lines) and $T=300$ K (dashed lines). Calculations ignoring the narrow gap at temperatures $T=50$ K (dashed-doted line) and $T=300$ K (solid line) are also presented. The relaxation frequency $\nu = 3\times10^{13}$ rad s^{-1} at $T=300$ K and $\nu = 2.3\times10^{13}$ rad s^{-1} at $T=50$ K.

Generally, both the finite-length-induced plasmonic effect and the curvature effect caused by the narrow gap must be jointly considered. Accordingly, Approach A was adopted, with the integral-equation method[6] used to compute $F_j(0,\omega,L)$. Equations (6.9) and (6.47) of Ref. 28 were employed to modify $\sigma_{zz}^{(j)}(\omega)$ for finite curvature.

As the curvature-induced energy gap $2E_g$ strongly depends on the chiral angle φ, an effective-medium description of the composite material should take metallic SWCNTs of all types and radius into account. However, as discussed by Tasaki *et al.* (p. 9305 in Ref. 32), the total contribution of the small gaps to the effective conductivity is negligible in comparison to the Drude term. We find that this is true only for high (room) temperature and for sufficiently long SWCNTs. In support of our contention, we present the calculated low-frequency spectra of $\mathrm{Re}(\sigma_{eff})$ of a composite material containing, for simplicity, only one type of metallic SWCNTs of identical length; hence, $N_1(L)=\delta(L-L_0)$ and $\tilde{n}_2=0$. For illustrative results, we chose the zigzag (27,0) SWCNTs as the inclusions, with $2E_g \simeq 9.1$ meV, that corresponds to the frequency of experimentally observed TCP.[18]

The computed spectra of $\mathrm{Re}(\sigma_{eff})/f$ are shown in Fig. 4 for $T=50$ K and $T=300$ K. The curvature effect is significant only at the lower temperature. At room temperature ($T=300$ K), the contribution of intraband transitions dominates

the contribution of the curvature effect, and the latter can be neglected. These results justify the description of the (room-temperature) experimental data presented in Fig. 3 by a theoretical model that neglects the curvature of SWCNTs.

The temperature dependence of σ_{eff} in the neighborhood of the TCP is determined by two mechanisms as follows:[33] the first is the decrease in ν with decreasing T, and the second is the change in the occupancies of the conduction and valence bands, as determined by the Fermi-distribution function of E_g.

At low temperature ($T=50$ K), the axial conductivity of an SWCNT is mostly determined by a contribution from the curvature effect that leads to a conductivity peak at the frequency $E_g/\pi\hbar$ for composite materials comprising sufficiently long SWCNTs; see the dotted line in Fig. 4(a). For shorter CNTs, the influence of the depolarization effect is comparable with the influence of the curvature effect—as may be seen by comparing the dotted and dashed-dotted lines in Fig. 4(b)—leading to a single terahertz peak at the frequency determined by both effects. The effective conductivity of a composite material comprising sufficiently short SWCNTs is fully determined by plasmonic effects and has a resonant peak corresponding to the first geometrical (antenna) resonance of short SWCNTs,[6] see Fig. 4(c).

IV. CONCLUSION

Thus, a finite-length-induced axial plasmonic effect and a curvature-induced narrow-gap effect do not offer mutually exclusive interpretations of the experimentally observed TCP. In general, for realistic composite materials containing narrow-gap SWCNTs, both mechanisms contribute simultaneously and cause the appearance only one terahertz peak. The combined influence is not merely superposition, either of the two can dominate but both must be accounted for in general.

To our knowledge, no direct experimental demonstration of the correlation of the TCP with the length of the SWCNTs has ever been reported. This may be so because the mechanism of axial depolarization for the existence of the TCP had hitherto not been identified. The first indications leading to this identification came in 2006.[6,19] Now, we have given here a comprehensive analysis of the effects of both *finite curvature* and *finite length* on the electromagnetic properties of SWCNTs in the terahertz regime—a theoretical developed which is hoped to stimulate experimental efforts.

In conclusion, we presented a theoretical model to explain a terahertz peak in the effective conductivity of a dilute and disordered composite material containing SWCNTs as inclusions. The model was applied to interpret available experimental data.[13–22] We determined that the dependences of the effective conductivity on the frequency and temperature arise from the combined action of two finite-size effects: (i) the modification of electron transport by the surface curvature of finite-radius SWCNTs and (ii) an axial depolarization effect due to the finite length of metallic SWCNTs.

ACKNOWLEDGMENTS

This research was partially supported by the International Bureau BMBF (Germany) under Project No. BLR 08/001, the Belarus Republican Foundation for Fundamental Research under Project No. F09MC-009, the EU FP7 CA-COMEL under Project No. FP7-247007, the ISTC under Project No. B-1708, the Charles Godfrey Binder Endowment at Penn State, and the alumni endowment funds of IIT Kanpur. The work of S.A.M. and G.Ya.S. was partially carried out during their stay at the Institut für Festkörperphusik, TU Berlin, and was supported by DAAD and DFG, respectively.

[1] S. Reich, C. Thomsen, and J. Maultzsch, *Carbon Nanotubes: Basic Concepts and Physical Properties* (Wiley-VCH, Berlin, Germany, 2004).
[2] G. Ya. Slepyan, S. A. Maksimenko, A. Lakhtakia, O. Yevtushenko, and A. V. Gusakov, Phys. Rev. B **60**, 17136 (1999).
[3] G. Miano and F. Villone, IEEE Trans. Antennas Propag. **54**, 2713 (2006).
[4] G. W. Hanson, IEEE Trans. Antennas Propag. **53**, 3426 (2005).
[5] P. J. Burke, S. Li, and Z. Yu, IEEE Trans. Nanotechnol. **5**, 314 (2006).
[6] G. Ya. Slepyan, M. V. Shuba, S. A. Maksimenko, and A. Lakhtakia, Phys. Rev. B **73**, 195416 (2006).
[7] A. M. Nemilentsau, G. Ya. Slepyan, and S. A. Maksimenko, Phys. Rev. Lett. **99**, 147403 (2007).
[8] M. V. Shuba, S. A. Maksimenko, and G. Ya. Slepyan, J. Comput. Theor. Nanosci. **6**, 2016 (2009).
[9] M. V. Shuba, S. A. Maksimenko, and A. Lakhtakia, Phys. Rev. B **76**, 155407 (2007).
[10] M. V. Shuba, G. Ya. Slepyan, S. A. Maksimenko, C. Thomsen, and A. Lakhtakia, Phys. Rev. B **79**, 155403 (2009).
[11] S. A. Maksimenko, G. Ya. Slepyan, A. M. Nemilentsau, and M. V. Shuba, Physica E **40**, 2360 (2008).
[12] A. Lakhtakia, G. Ya. Slepyan, S. A. Maksimenko, A. V. Gusakov, and O. M. Yevtushenko, Carbon **36**, 1833 (1998).
[13] A. Ugawa, A. G. Rinzler, and D. B. Tanner, Phys. Rev. B **60**, R11305 (1999).
[14] B. Ruzicka, L. Degiorgi, R. Gaal, L. Thien-Nga, R. Bacsa, J.-P. Salvetat, and L. Forro, Phys. Rev. B **61**, R2468 (2000).
[15] M. E. Itkis, S. Niyogi, M. E. Meng, M. A. Hamon, H. Hu, and R. C. Haddon, Nano Lett. **2**, 155 (2002).
[16] T.-I. Jeon, K.-J. Kim, C. Kang, S.-J. Oh, J.-H. Son, K. H. An, D. J. Bae, and Y. H. Lee, Appl. Phys. Lett. **80**, 3403 (2002).
[17] H. Hu, B. Zhao, M. A. Hamon, K. Kamaras, M. E. Itkis, and R. C. Haddon, J. Am. Chem. Soc. **125**, 14893 (2003).
[18] F. Borondics, K. Kamarás, M. Nikolou, D. B. Tanner, Z. H. Chen, and A. G. Rinzler, Phys. Rev. B **74**, 045431 (2006).
[19] N. Akima, Y. Iwasa, S. Brown, A. M. Barbour, J. Cao, J. L. Musfeldt, H. Matsui, N. Toyota, M. Shiraishi, H. Shimoda, and O. Zhou, Adv. Mater. **18**, 1166 (2006).
[20] C. Kang, I. H. Maeng, S. J. Oh, S. C. Lim, K. H. An, Y. H. Lee, and J.-H. Son, Phys. Rev. B **75**, 085410 (2007).
[21] T. Kampfrath, L. Perfetti, K. von Volkmann, C. M. Aguirre, P.

Desjardins, R. Martel, C. Frischkorn, and M. Wolf, Phys. Status Solidi B **244**, 3950 (2007).
[22] T. Kampfrath, K. von Volkmann, C. M. Aguirre, P. Desjardins, R. Martel, M. Krenz, C. Frischkorn, M. Wolf, and L. Perfetti, Phys. Rev. Lett. **101**, 267403 (2008).
[23] F. L. Shyu and M. F. Lin, J. Phys. Soc. Jpn. **71**, 1820 (2002).
[24] C. L. Kane and E. J. Mele, Phys. Rev. Lett. **78**, 1932 (1997).
[25] A. D. Yaghjian, Proc. IEEE **68**, 248 (1980).
[26] P. C. Waterman and R. Truell, J. Math. Phys. **2**, 512 (1961).
[27] A. Lakhtakia, Int. J. Electron. **75**, 1243 (1993).
[28] S. A. Maksimenko and G. Ya. Slepyan, in *Electromagnetic Fields in Unconventional Materials and Structures*, edited by O. N. Singh and A. Lakhtakia (Wiley, New York, 2000), pp. 217–255.
[29] M. S. Fuhrer, M. L. Cohen, A. Zettl, and V. Crespi, Solid State Commun. **109**, 105 (1999).
[30] P. Petit, E. Jouguelet, J. E. Fischer, A. G. Rinzler, and R. E. Smalley, Phys. Rev. B **56**, 9275 (1997).
[31] L. Novotny and B. Hecht, *Principles of Nano-Optics* (Cambridge University Press, Cambridge, United Kingdom, 2006).
[32] S. Tasaki, K. Maekawa, and T. Yamabe, Phys. Rev. B **57**, 9301 (1998).
[33] E. M. Lifshitz and L. P. Pitaevskii, *Statistical Physics: Theory of the Condensed State* (Pergamon, New York, 1980).